

Article

Removal of Disinfection By-Products Precursor (Humic Acid) by Graphene-Silica Composites

Siqi Chen, Shanze Shang, Qi Zhao, Shaojie Zhang and Wu Yang *

School of Environment, Northeast Normal University, Changchun 130117, China; chensq698@nenu.edu.cn (S.C.); sss1078915696@163.com (S.S.); zhaoq926@nenu.edu.cn (Q.Z.); zhangsj1215@163.com (S.Z.)

* Correspondence: yangw104@nenu.edu.cn; Tel.: +86-181-6686-7927

Abstract: Graphene-silica (RGO-SiO₂) was successfully synthesized by a simple hydrothermal method. The composites were used to study the adsorption properties of humic acid and disinfection by-product precursors in natural surface water. Compared with reduced graphene oxide (RGO), the specific surface area of the composites doped with silica (SiO₂) increased by 31.2% to 259.43 m²/g. RGO-SiO₂ could achieve 66.91% adsorption of humic acid (HA), while the maximum adsorption of HA on RGO-SiO₂ reached 925.91 mg/g. The adsorption and removal rates of HA by RGO-SiO₂ were significantly higher than those of RGO. The whole adsorption process was in accordance with the quasi-secondary kinetic model, the Langmuir isothermal adsorption model. RGO-SiO₂ has good adsorption performance for organic matter of different water qualities. RGO-SiO₂ has a better removal ability for hydrophobic organics than hydrophilic and nitrogenous organics. The adsorbent was reusable, and the organic removal efficiency of RGO-SiO₂ decreased insignificantly after four cycles.

Keywords: adsorption; disinfection byproducts; humic acid; RGO-SiO₂ composite



Citation: Chen, S.; Shang, S.; Zhao, Q.; Zhang, S.; Yang, W. Removal of Disinfection By-Products Precursor (Humic Acid) by Graphene-Silica Composites. *Water* **2022**, *14*, 1178. <https://doi.org/10.3390/w14071178>

Academic Editor: Paola Verlicchi

Received: 7 February 2022

Accepted: 17 March 2022

Published: 6 April 2022

Publisher's Note: MDPI stays neutral with regard to jurisdictional claims in published maps and institutional affiliations.



Copyright: © 2022 by the authors. Licensee MDPI, Basel, Switzerland. This article is an open access article distributed under the terms and conditions of the Creative Commons Attribution (CC BY) license (<https://creativecommons.org/licenses/by/4.0/>).

1. Introduction

Drinking water disinfection is an indispensable process that improves water quality and prevents water-borne diseases. However, the resulting harmful disinfection byproducts (DBPs) are increasingly becoming a focus of hot issues. Certain DBPs have been proven to have very severe carcinogenic, teratogenic, and mutagenic effects on laboratory animals in toxicological investigations. Individuals who are exposed to chlorinated surface waters for a long time have a slightly elevated risk of bladder, colon, and rectal cancers, according to epidemiological studies, and will also affect reproduction and development [1].

In view of DBPs, there exist potential health risks, and controlling DBPs has become imperative. Controlling DBPs' precursors is considered to be the most effective DBPs control measure because this method will not only not produce other DBPs in the treatment process but can also make use of the existing treatment facilities [2]. Natural organic matter (NOM) can be found in large quantities in both surface and shallow groundwater. Humic substances are the main component of NOM and account for 50–90 percent [3]. Humic compounds are mostly made up of humic acid (HA), and too much of it in drinking water can cause major environmental and health issues, especially in the process of disinfection, where HA can react with disinfectant to generate carcinogenic DBPs [4]. At present, the main control methods of these DBPs precursors are enhanced coagulation [5], membrane filtration [6], advanced oxidation [7], magnetic ion exchange resin [8], and adsorption [9]. Due to its economic efficiency, simple operation, and environment-friendly process, adsorption has been thought of as the frequent method for removing NOM [10].

Graphene (GO) is the first actual 2D carbon material, as well as artificial, and is known as the world's thinnest material [11]. Graphene has piqued the scientific community's curiosity since it was discovered in 2004. In the field of water environment research, GO is

commonly utilized to adsorb heavy metal ions, inorganic anions, dyes, endocrine disruptors, medicines, personal care items, and natural organic matter, among other things [12]. In this study, silica (SiO_2) was combined with graphene to weaken mutual aggregation between graphene sheets, resulting in a graphene-silica (RGO- SiO_2) composite material with a high specific surface area and outstanding adsorption capacity. The goals of this study are to investigate the adsorption properties of composites for NOM and perform thermodynamic and kinetic fitting, as well as to apply the composites to NOM adsorption in real water bodies and to explore its reusability.

2. Materials and Methods

2.1. Materials and Reagents

Graphite was bought from Qingdao Tianhe Graphite Co., Ltd. (Qingdao, China). Analytical reagent grade of potassium permanganate was obtained from Sinopharm Chemical Reagent Co., Ltd. (Shanghai, China). Analytical reagent grades of sulfuric acid, hydrogen peroxide, anhydrous ethanol, ammonia water, and ethyl orthosilicate (TEOS) were purchased from Beijing Chemical Factory (Beijing, China). Deionized (DI) water was used to produce all the solutions. Dissolving HA was purchased from Chengdu West Asia Chemical Co., Ltd. (Chengdu, China), in DI water, and yielded the initial HA solution.

2.2. Preparation and Characterization of RGO- SiO_2

A modified Hummers method of pressurized oxidation was used to synthesize GO from natural graphite (Qingdao Tianhe Graphite Co., Ltd., Qingdao, China) [13]. RGO and RGO- SiO_2 were synthesized by a hydrothermal process [14]. GO, DI water, and anhydrous ethanol were mixed in proportion in a 500 mL flask, the pH of the mixture was adjusted to 10.0 ± 0.1 with ammonia solution, and then TEOS was added. The liquid was mixed for 24 h at room temperature before being placed into a Teflon reactor, which was then covered and secured with a stainless steel autoclave. For 24 h, the autoclave was held at 453 K in an oven. After that, the resulting product was washed multiple times with anhydrous ethanol and DI water before being dried at 338 K. To obtain a decreased RGO- SiO_2 , the dry product was ground into powder.

The surface morphology of RGO and RGO- SiO_2 was examined by SEM (FEI, XL30-ESEM). Fourier transform infrared (FT-IR) spectroscopy was used to analyze the surface characteristics and composition of RGO and RGO- SiO_2 utilizing KBr pellets in the range $500\text{--}4000\text{ cm}^{-1}$ on a ThermoFisher Nicolet 6700 FT-IR spectrometer. X-ray diffraction (XRD) measurements were obtained with a Bruker, SMART APEXII CCD X-ray diffractometer (Philips) utilizing CuK α radiation and a scanning range of $5\text{--}50^\circ$. The Brunauer-Emmett-Teller (BET) surface area of RGO and RGO- SiO_2 were measured using N_2 adsorption and desorption (Micromeritics ASAP 2020) across a relative pressure range of 0.0955 to 0.993 at 77 K.

2.3. Adsorption Tests

Adsorption of HA onto RGO- SiO_2

At room temperature (293 K), all the batch adsorption studies were carried out, all the adsorption solutions' pH were controlled at 7.0 ± 0.1 , except especially noted.

Kinetic experiment: HA solutions of different concentrations were prepared, 30 mg RGO- SiO_2 was dispersed into the initial concentration of HA solution, and was 100, 300, and 500 mg/L with 0.001 M CaCl_2 (100 mL), respectively, and the solution was shaken for 240 min at 300 rpm using a magnetic stirrer. An amount of 4 mL of the mixture was withdrawn and filtrated with a $0.45\text{ }\mu\text{m}$ filter at different time intervals for measuring the residual HA concentration at a wavelength of 254 nm.

Comparison of HA adsorption on RGO- SiO_2 and RGO: To compare the adsorption capacity of RGO- SiO_2 and RGO, RGO- SiO_2 and RGO at an initial concentration of 300 mg/L were put into 300 mg/L of HA solution with 0.001 M of CaCl_2 (100 mL), and the mixtures were shaken at 300 rpm with a magnetic stirrer for 240 min and sampled at various time

intervals. The HA concentrations were determined at 254 nm using a Universal T6 UV-vis spectrophotometer after the samples were filtered using a 0.45 μm filter membrane.

Effect of adsorbent dosage: 10–40 mg of RGO-SiO₂ was added to 100 mL, 300 mg/L of HA solution containing 0.001 M of CaCl₂, and the samples were taken at different time intervals from 5 to 240 min. The HA concentrations were determined at 254 nm using a Universal T6 UV-vis spectrophotometer after the samples were filtered using a 0.45 μm filter membrane.

Effect of pH: 6 mg RGO-SiO₂ was added into the initial concentration of HA, the solution was 300 mg/L with 0.001 M of CaCl₂ (20 mL), and 0.1 M of NaOH or HCl solution, which was used to change the pH value from 4.0 ± 0.1 to 10.0 ± 0.1 . The mixture was shaken at 300 rpm for 1 h and then the value of UV₂₅₄ was measured. The experiment was conducted three times.

Effect of water matrix: Three water samples were collected from the Landscape Lake of Northeast Normal University's Jingyue Campus (denoted as JY), the Yitong River in Changchun City (denoted as YT), and the reclaimed water from Changchun Nanjiao Sewage Treatment Plant (denoted as NJ). The studies were repeated three times with 90 mg RGO-SiO₂ added to 150 mL water samples from JY, YT, and NJ, respectively.

Reuse of RGO-SiO₂: 90 mg of RGO-SiO₂ was added to 150 mL of the YT water sample for adsorption, and after saturation, the material was stirred for 12 h with 150 mL of absolute ethanol, and then washed with pure water multiple times before being dried in a 60 °C oven. For adsorption studies, the dried RGO-SiO₂ was used again. The experiments were repeated 3 times.

3. Results

3.1. Characterization of RGO-SiO₂

3.1.1. Scanning Electron Microscope Analysis

SEM images of RGO (Figure 1a,c) and RGO-SiO₂ (Figure 1b,d) under different magnifications are shown in Figure 1. From a and c, we can see that RGO is a petaloid cluster, the surface of RGO exists as a fold and occurs as a stack between graphene layers. It is mainly caused by the inevitable van der Waals force between graphene layers. From b and d, we can observe that RGO-SiO₂ presents a layer structure and small SiO₂ nanoparticles are homogeneously distributed on graphene sheets, which present as a white spherical shape. The decorated SiO₂ nanoparticles could act as a spacer to decrease the interaction between graphene layers, thus increasing the specific surface area of composite [15].

3.1.2. Fourier Transform Infrared Spectroscopy Analysis

ATR-FTIR spectrum of GO (a), RGO (b), and RGO-SiO₂ (c) are shown in Figure 2. Compared with graphite, the ATR-FTIR spectra of GO following oxidation shows multiple distinct peaks of various carbon-oxygen functional groups: C-O, C-O-C, C-OH, C=C, C=O, O-H, which indicates that the graphite was fully oxidized and prepared GO successfully [13]. RGO compares with GO and shows that the functional groups are significantly weakened and even disappeared, showing that RGO prepared by the hydrothermal process has a high degree of reduction. RGO-SiO₂ compares with RGO and demonstrates that there are two new absorption peaks at 1101 cm^{-1} and 955 cm^{-1} that imply the stretching vibration peak of Si-O-Si and Si-OH, respectively [16,17], demonstrating that SiO₂ was successfully coated onto RGO. Moreover, The C=O group has disappeared at 1725 cm^{-1} , showing that the oxygen that contains functional groups of RGO-SiO₂ that are prepared by the hydrothermal method are largely removed. There is only a small part of the polar group, thus this increases its hydrophobicity [18].

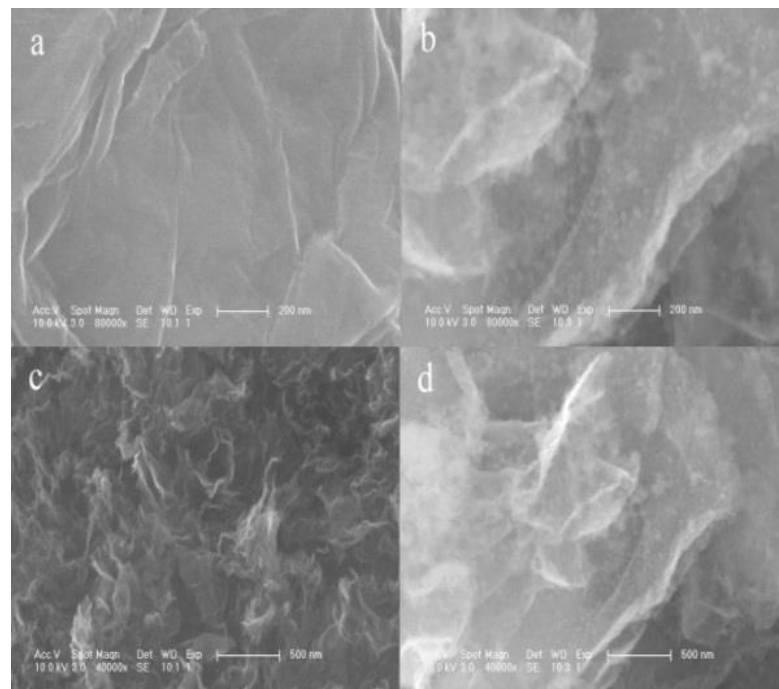


Figure 1. SEM images of graphene oxide (RGO) (a,c) and graphene-silica (RGO-SiO₂) (b,d) under different magnifications.

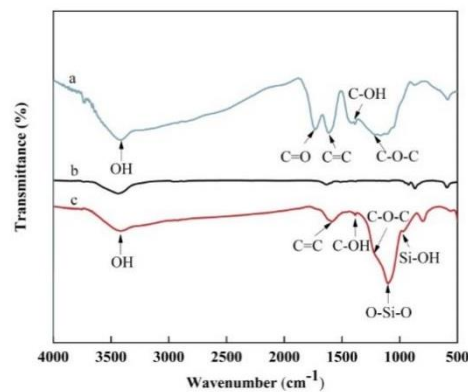


Figure 2. FT-IR spectrum of graphene GO (a), RGO (b), and RGO-SiO₂ (c).

3.1.3. X-ray Diffraction Analysis

XRD patterns of RGO (a) and RGO-SiO₂ (b) are shown in Figure 3. There is a very weak yet broad diffraction peak at $2\theta = 20\sim 30^\circ$, indicating that graphene occurs as a stack in the drying process [13]. The diffraction peak of RGO-SiO₂ occurs at $2\theta = 20\sim 30^\circ$, which is narrower than RGO, showing that the presence of SiO₂ effectively avoids the stack of the bulk of the graphene layers.

3.1.4. BET Specific Surface Area Analysis

Figure 4 shows the nitrogen adsorption–desorption isotherms for RGO (a) and RGO-SiO₂ (b). The particular surface area of RGO computed by the BET model is 177.35 m²/g, a significant difference from the theoretical value of the graphene surface area (2600 m²/g). Because of the unavoidable van der Waals force between single graphene layers, the reason could be related to a partial exfoliation of GO and severe aggregation of graphene layers during the reduction process [19]. The specific surface area of RGO-SiO₂ is 256.72 m²/g, larger than RGO, and might be attributed to the presence of SiO₂ increasing the spacing between graphene layers, reducing the interactions between graphene layers, and increasing the specific surface area.

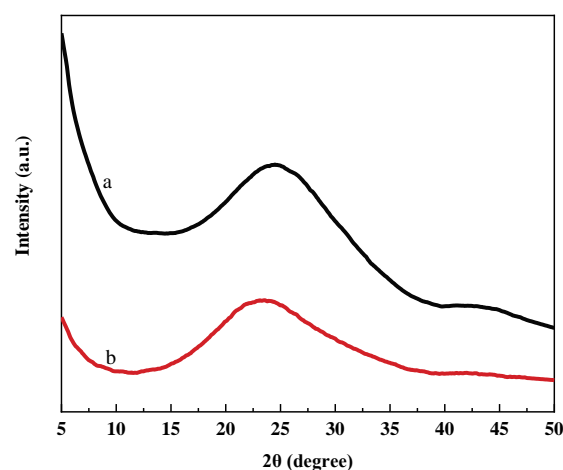


Figure 3. XRD patterns of RGO (a) and RGO-SiO₂ (b).

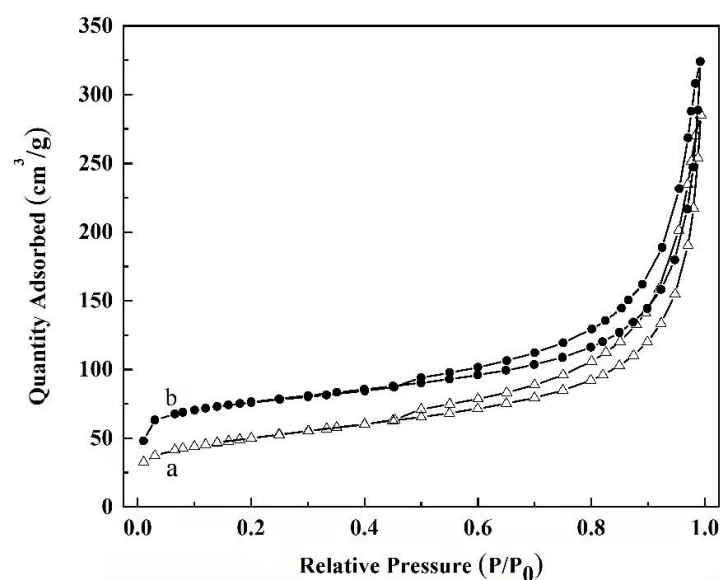


Figure 4. Nitrogen adsorption–desorption isotherm for RGO (a) and RGO-SiO₂ (b).

3.2. Adsorption of HA onto RGO-SiO₂

3.2.1. Effect of Initial Concentration of HA Solutions

The effect of the initial concentration of HA on the adsorption of HA onto RGO-SiO₂ is illustrated in Figure 5. Adsorption can rapidly occur within the first of 10 min and reach adsorption equilibrium at around 60 min. The adsorption amounts of HA onto RGO-SiO₂ increase from 331.3 mg/g to 493.2 mg/g as the initial concentration increases. When the initial concentration of HA is higher than 300 mg/L, the adsorption amounts reach the maximum, nevertheless, as the initial concentration is increased further, the adsorption amounts do not change much.

3.2.2. Comparison of HA Adsorption on RGO-SiO₂ and RGO

Figure 6 shows the comparison of RGO and RGO-SiO₂. The adsorption and removal of HA by RGO-SiO₂ is higher than that by RGO, which is mainly due to the unavoidable force of RGO in the preparation process and the occurrence of serious agglomeration, which makes its specific surface area lower and leads to low adsorption efficiency; while the presence of SiO₂ increases the spacing of graphene sheets and reduces the aggregation between graphene, which makes the specific surface area increase and provides more adsorption sites and higher adsorption efficiency.

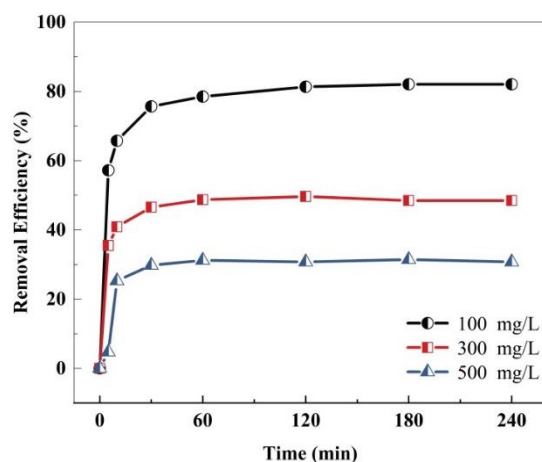


Figure 5. Effect of initial humic acid (HA) concentration on the adsorption of HA onto RGO-SiO₂.

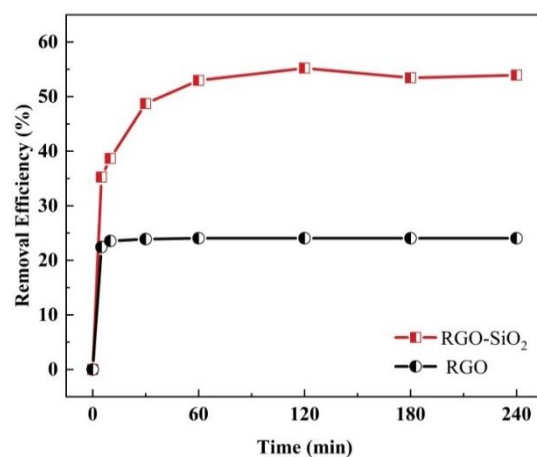


Figure 6. Adsorption of RGO and RGO-SiO₂ on HA.

3.2.3. Effect of Adsorbent Dosage

Figure 7 illustrates the influence of adsorbent dose on the adsorption of HA by composites. The removal of HA by RGO-SiO₂ increased from 27.31% to 66.91% with increasing the amount of adsorbent (100–400 mg/L). The increase in adsorption efficiency is due to an increase in the amount of adsorbent employed and the number of accessible adsorption sites, which results in an increase in the adsorption surface area. For the following studies, an adsorbent dosage of 300 mg/L was used due to the dual consideration of the adsorption removal rate and adsorption capacity.

3.2.4. Effect of pH

The effect of pH on the adsorption of HA onto RGO-SiO₂ can be seen in Figure 8. With the increase in pH, the adsorption removal efficiencies of HA onto RGO-SiO₂ decrease from 83.5% to 59.0%. The main reasons are as follows: The lower pH, the higher the surface positive charge density of RGO-SiO₂ and it might make it easier for negatively charged HA to stick to the surface, thus increasing the adsorption efficiency. As pH increased, the dissociation of the functional groups -COOH and -COH to -COO⁻ and -CO⁻ increased, resulting in RGO-SiO₂ being negatively charged. The adsorption capacity was reduced due to the electrostatic repulsion interaction between the negative charges on RGO-SiO₂ and HA [17]. At lower pH, HA can be found in a spherical shape, but at higher pH, it can be found in a linear or stretched structure. The smaller the molecule volume, the easier it is to adsorb [20].

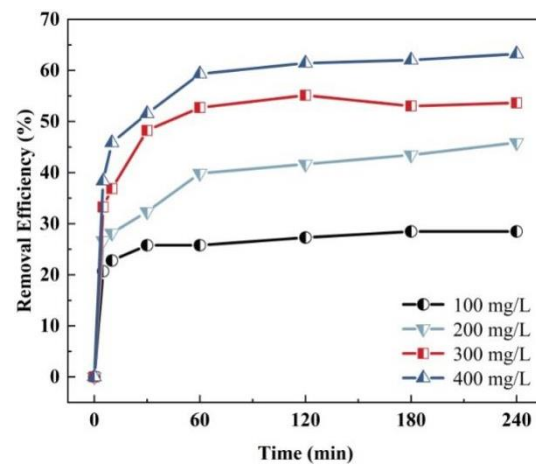


Figure 7. Effect of adsorbent dosage on HA adsorption by RGO-SiO₂.

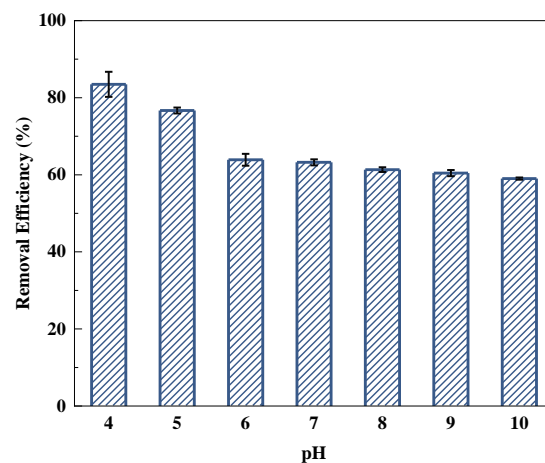


Figure 8. Effect of pH on the adsorption of HA onto RGO-SiO₂.

3.2.5. Adsorption Kinetics

Many different kinetic models have been proposed to explore the adsorption mechanism. In this study, two different kinetic models are applied to obtain the most matched one with the experimental data: pseudo-first-order kinetic models and pseudo-second-order kinetic models [4]. The linear forms of the pseudo-first-order and pseudo-second-order kinetic models are expressed as Equations (1) and (2), respectively:

$$\ln(q_e - q_t) = \ln q_e - k_1 t \quad (1)$$

$$\frac{t}{q_t} = \frac{1}{k_2 q_e^2} + \frac{t}{q_e} \quad (2)$$

where q_e and q_t are the equilibrium and time t adsorption capacities ($\text{mg} \cdot \text{g}^{-1}$), respectively, k_1 is the pseudo-first-order rate constant (min^{-1}), k_2 ($\text{g}/\text{mg} \cdot \text{min}$) is the pseudo-second-order rate constant.

Adsorption kinetic parameters of the adsorption of HA onto RGO-SiO₂ at different initial concentrations are shown in Table 1. Under different experimental conditions, HA adsorbed on RGO-SiO₂ and the quasi-secondary kinetic fits on RGO-SiO₂, as shown in Figure 9. As can be seen from Table 1, the value of correlation coefficient (R^2) of pseudo-first-order kinetic models is smaller than pseudo-second-order kinetic models' which are close to 1. Additionally, the theoretical values of q_e are close to the value of q_e obtained at experimental conditions, indicating that pseudo-second-order kinetic models have a good agreement with the experimental data; the adsorption of HA onto RGO-SiO₂ follows

pseudo-second-order kinetic models in the whole adsorption time, and adsorption is mainly chemisorption [4].

Table 1. Comparison of the pseudo-first-order and pseudo-second-order kinetic models for the adsorption of HA onto RGO-SiO₂.

C _{HA} (mg/L)	Pseudo-First-Order			Pseudo-Second-Order		
	R ²	q _e (mg/g)	K ₁ (min ⁻¹)	R ²	q _e (mg/g)	K ₂ (g/(mg·min))
100	0.9567	85.71	0.028	0.9969	335.97 (331.27)	0.0029
300	0.3176	71.51	0.0077	0.9994	490.20 (483.65)	0.0016
500	0.5266	82.92	0.0083	0.9992	502.51 (493.17)	0.0015

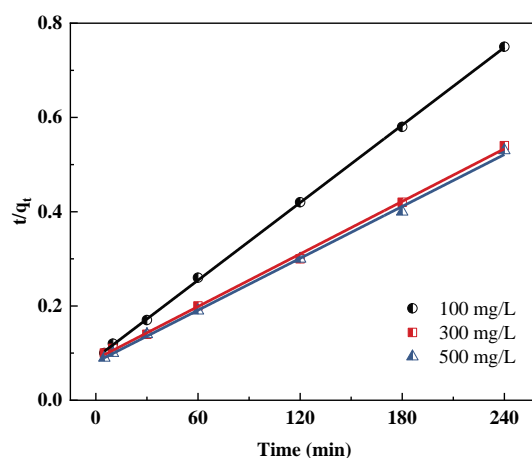


Figure 9. Linear plots of a pseudo-second-order kinetic model for the adsorption of HA onto RGO-SiO₂.

3.2.6. Adsorption Isotherm

Two of the most often used models, Langmuir and Freundlich [20], were chosen to match the experimental data in this work. The linear form of Langmuir and Freundlich is as follows:

$$\frac{1}{q_e} = \frac{1}{k_L C_e} + \frac{a_L}{k_L}$$

$$\log q_e = \log k_F + \frac{\log C_e}{n}$$

where C_e is the equilibrium concentration of adsorbate (mg/L), q_e is the adsorption amount at equilibrium (mg/g), a_L (L/mg), k_L (L/g), k_F ((mg/g) (mg/L)⁻¹/n) and n are constants.

HA adsorbed in RGO-SiO₂ on the Langmuir isotherm fitting line is shown in Figure 10. Table 2 shows the Langmuir and Freundlich isotherm constants for the adsorption of HA onto RGO-SiO₂, from which we can deduce that the Langmuir model's R² value is higher than the Freundlich model's, implying that the Langmuir model fits better and that the adsorption process is monolayer [21].

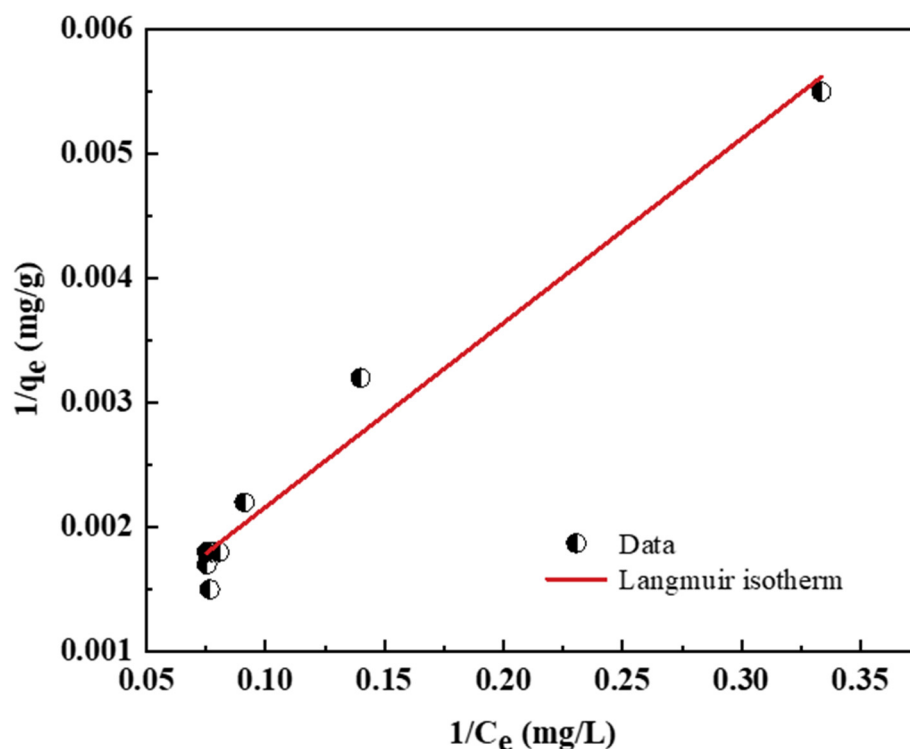


Figure 10. Isotherm data and modeling for the adsorption of HA on RGO-SiO₂.

Table 2. Langmuir and Freundlich isotherm constants for the adsorption of HA onto RGO-SiO₂.

Langmuir			Freundlich		
R ²	k _L (L/g)	a _L (L/mg)	R ²	k _F ((mg/g)(g/L) ^{-1/n})	n
0.9712	95.24	0.13	0.8766	174.58	3.89

3.3. Adsorption of Organic Matter in Surface Water onto RGO-SiO₂

3.3.1. Effect of Water Matrix

Table 3 lists the basic water quality parameters of three kinds of raw water. The adsorption of NOM onto RGO-SiO₂ under different water qualities is shown in Figure 11. After disinfection, three raw water samples detected eight kinds of DBPs: Trichloromethane (TCM), trichloroacetonitrile (TCAN), bromodichloromethane (BDCM), halo acetaldehydes (CH), trichloroacetic acid (TCAA), dichloroacetic acid (DCAA), bromo dichloroacetic acid (BDCAA) and dibromoacetic acid (DBAA). RGO-SiO₂ has a good adsorption capability for three kinds of water samples. The UV₂₅₄ removal efficiency is 71.8~75.7%, dissolved organic carbon (DOC) removal efficiency is 47.5~51.2%, TCMFP, TCANFP, BDCMFP, and CHFP are 33.1~43.7%, 0.9~4.5%, 0.8~20.4%, and 75.9~84.6%, respectively, and DCAAFP, TCAAFP, BDCAAFP, and DBAAFP is 57.7~63.0%, 69.1~71.9%, 67.8~69.9%, and 17.4~27.4%, respectively.

Table 3. Basic water quality parameters of experiment water.

Water Sample	pH	Turbidity (NTU)	UV ₂₅₄ (cm ⁻¹)	DOC (mg/L)	SUVA (L/mg/m)
YT	7.94	19.7	0.123	7.416	1.66
NJ	7.71	4.6	0.131	8.203	1.60
JY	7.40	21.4	0.079	5.337	1.48

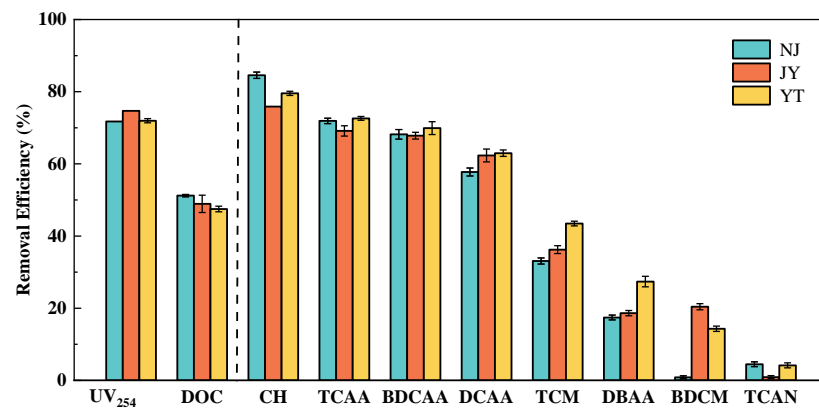


Figure 11. Effect of different water qualities on the adsorption of natural organic matter (NOM) onto RGO-SiO₂.

The removal capacity of RGO-SiO₂ on haloacetic acid (HAAsFP) is higher than trihalomethane (THMsFP), which is owing to the precursor of HAAs being mainly hydrophobic organic compounds [22]. The adsorption capacity of RGO-SiO₂ on hydrophobic organic compounds in water is stronger.

3.3.2. Reuse of RGO-SiO₂

In this study, absolute ethyl alcohol was used as a desorbing agent. The RGO-SiO₂, after desorption, was repeatedly used for the adsorption experiments of organic matter in surface water. The removal efficiency of NOM in the surface water of regenerated adsorbent is given in Figure 12. The adsorption removal effectiveness of NOM onto RGO-SiO₂ is observed to be slightly reduced after three cycles, and no obvious decrease after the next cycle, which indicates that the regenerated RGO-SiO₂ retains its outstanding NOM adsorption removal effectiveness in surface water, and the adsorbent can be reused [10].

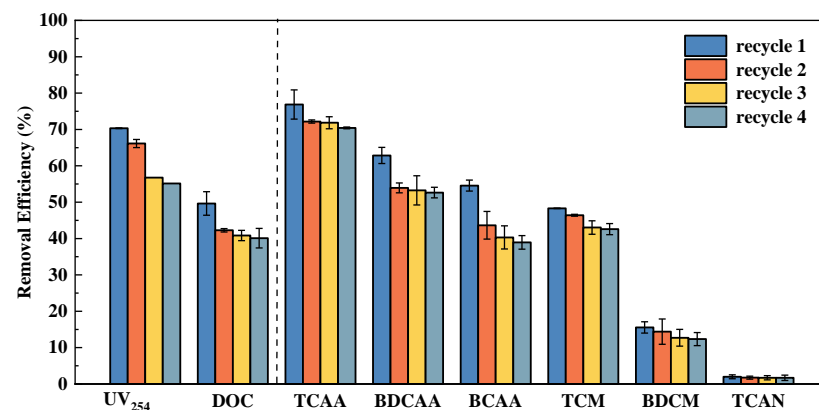


Figure 12. Reuse of RGO-SiO₂.

4. Conclusions

The SiO₂ coating on the RGO surface lowers graphene layer interactions while increasing specific surface area and adsorption capacity. Throughout the process of HA adsorption, adsorption can occur rapidly in the first 10 min and reach equilibrium in around 60 min. As the initial concentration of HA decreases and the pH value increases, the adsorption removal of HA on RGO-SiO₂ increases, and the adsorption performance of RGO-SiO₂ is higher than that of a single RGO for the whole adsorption time. The adsorption behavior of HA on RGO-SiO₂ may be effectively described by the pseudo-second-order kinetic model and the Langmuir model, and the adsorption of HA on RGO-SiO₂ belongs to monolayer adsorption and chemisorption. In the adsorption process of natural organic matter on RGO-SiO₂ in surface water, RGO-SiO₂ has good adsorption performance of UV₂₅₄, DOC,

and DBPsFP on water samples with different water qualities, and the removal ability of HAAsFP is stronger than that of THMsFP. The adsorption and removal ability of RGO-SiO₂ does not decrease significantly after several cycles, and the adsorbent RGO-SiO₂ can quickly adsorb NOM in water, and its preparation method is simple and low cost with a high removal efficiency.

Author Contributions: Conceptualization, S.C. and W.Y.; methodology, S.C. and W.Y.; formal analysis, S.S.; resources, Q.Z. and S.Z.; data curation, S.C. and S.S.; writing—original draft preparation, S.C.; writing—review and editing, W.Y.; supervision, W.Y.; funding acquisition, W.Y. All authors have read and agreed to the published version of the manuscript.

Funding: This research was funded by [the Fundamental Research Funds for the Central Universities] grant number [2412019FZ020] and [the National Key Research and Development Program of China] grant number [2019YFE0117900].

Institutional Review Board Statement: Not applicable.

Informed Consent Statement: Not applicable.

Data Availability Statement: Not applicable.

Acknowledgments: The authors wish to thank Huan Zhou for supporting the real water sample.

Conflicts of Interest: The authors declare no conflict of interest.

References

1. Boorman, G.A.; Dellarco, V.; Dunnick, J.K.; Chapin, R.E.; Hunter, S.; Hauchman, F.; Gardner, H.; Cox, M.; Sills, R.C. Drinking water disinfection byproducts: Review and approach to toxicity evaluation. *Environ. Health Perspect.* **1999**, *107*, 207–217. [[PubMed](#)]
2. Bond, T.; Goslan, E.H.; Parsons, S.A.; Jefferson, B. Treatment of disinfection by-product precursors. *Environ. Technol.* **2011**, *32*, 1–25. [[CrossRef](#)] [[PubMed](#)]
3. Bhatnagar, A.; Sillanpaa, M. Removal of natural organic matter (NOM) and its constituents from water by adsorption—A review. *Chemosphere* **2017**, *166*, 497–510. [[CrossRef](#)] [[PubMed](#)]
4. Doulia, D.; Leodopoulos, C.; Gimouhopoulos, K.; Rigas, F. Adsorption of humic acid on acid-activated Greek bentonite. *J. Colloid Interface Sci.* **2009**, *340*, 131–141. [[CrossRef](#)]
5. Wang, P.; Ding, S.K.; Xiao, R.; An, G.Y.; Fang, C.; Chu, W.H. Enhanced coagulation for mitigation of disinfection by-product precursors: A review. *Adv. Colloid Interface Sci.* **2021**, *296*, 19. [[CrossRef](#)]
6. Siddiqui, M.; Amy, G.; Ryan, J.; Odem, W. Membranes for the control of natural organic matter from surface waters. *Water Res.* **2000**, *34*, 3355–3370. [[CrossRef](#)]
7. Toor, R.; Mohseni, M. UV-H₂O₂ based AOP and its integration with biological activated carbon treatment for DBP reduction in drinking water. *Chemosphere* **2007**, *66*, 2087–2095. [[CrossRef](#)]
8. Mergen, M.R.D.; Jefferson, B.; Parsons, S.A.; Jarvis, P. Magnetic ion-exchange resin treatment: Impact of water type and resin use. *Water Res.* **2008**, *42*, 1977–1988. [[CrossRef](#)]
9. Kim, J.K.; Kang, B.S. DBPs removal in GAC filter-adsorber. *Water Res.* **2008**, *42*, 145–152. [[CrossRef](#)]
10. Wang, J.; Han, X.; Ma, H.; Ji, Y.; Bi, L. Adsorptive removal of humic acid from aqueous solution on polyaniline/attapulgite composite. *Chem. Eng. J.* **2011**, *173*, 171–177. [[CrossRef](#)]
11. Novoselov, K.S.; Geim, A.K.; Morozov, S.V.; Jiang, D.; Zhang, Y.; Dubonos, S.V.; Grigorieva, I.V.; Firsov, A.A. Electric field effect in atomically thin carbon films. *Science* **2004**, *306*, 666–669. [[CrossRef](#)] [[PubMed](#)]
12. Meng, L.; Sun, Y.; Gong, H.; Wang, P.; Qiao, W.C.; Gan, L.; Xu, L.J. Research progress of the application of graphene-based materials in the treatment of water pollutants. *New Carbon Mater.* **2019**, *34*, 220–237. [[CrossRef](#)]
13. Bao, C.L.; Song, L.; Xing, W.Y.; Yuan, B.; Wilkie, C.A.; Huang, J.; Guo, Y.; Hu, Y. Preparation of graphene by pressurized oxidation and multiplex reduction and its polymer nanocomposites by masterbatch-based melt blending. *J. Mater. Chem.* **2012**, *22*, 6088. [[CrossRef](#)]
14. Zhou, X.; Shi, T. One-pot hydrothermal synthesis of a mesoporous SiO₂-graphene hybrid with tunable surface area and pore size. *Appl. Surf. Sci.* **2012**, *259*, 566–573. [[CrossRef](#)]
15. Wu, Y.; Luo, H.; Wang, H.; Wang, C.; Zhang, J.; Zhang, Z. Adsorption of hexavalent chromium from aqueous solutions by graphene modified with cetyltrimethylammonium bromide. *J. Colloid Interface Sci.* **2013**, *394*, 183–191. [[CrossRef](#)] [[PubMed](#)]
16. Liu, Q.; Shi, J.B.; Sun, J.T.; Wang, T.; Zeng, L.; Jiang, G. Graphene and graphene oxide sheets supported on silica as versatile and high-performance adsorbents for solid-phase extraction. *Angew. Chem.* **2011**, *50*, 6035–6039. [[CrossRef](#)]
17. Hao, L.Y.; Song, H.J.; Zhang, L.C.; Wan, X.; Tang, Y.; Lv, Y. SiO₂/graphene composite for highly selective adsorption of Pb(II) ion. *J. Colloid Interface Sci.* **2012**, *369*, 381–387. [[CrossRef](#)]

18. Wang, J.; Chen, Z.; Chen, B. Adsorption of polycyclic aromatic hydrocarbons by graphene and graphene oxide nanosheets. *Environ. Sci. Technol.* **2014**, *48*, 4817–4825. [[CrossRef](#)]
19. Xu, J.; Wang, L.; Zhu, Y. Decontamination of Bisphenol A from Aqueous Solution by Graphene Adsorption. *Langmuir ACS J. Surf. Colloids* **2012**, *28*, 8418–8425. [[CrossRef](#)]
20. Jones, M.N.; Bryan, N.D. Colloidal properties of humic substances. *Adv. Colloid Interface Sci.* **1998**, *78*, 1–48. [[CrossRef](#)]
21. Shaker, A.M.; Komy, Z.R.; Heggy, S.E.; El-Sayed, M.E. Kinetic study for adsorption humic acid on soil minerals. *J. Phys. Chem. A* **2012**, *116*, 10889–10896. [[CrossRef](#)] [[PubMed](#)]
22. Wang, J.; Ding, S.; Zheng, C.; Ma, H.; Ji, Y. Efficient removal of humic acid in aqueous solution using polyaniline adsorbent. *Desalination Water Treat.* **2012**, *40*, 92–99. [[CrossRef](#)]